Parametric Design of Conforming Joints for Thin-Shell Coilable Structures

Daniel-Alexander Türk* and Sergio Pellegrino†
California Institute of Technology, Pasadena, CA, 91125

This paper addresses the problem of designing and building structural connections (joints) for ultra-thin shells employed in large coilable structures for space applications. A conforming joint design concept for ladder-type coilable thin shells is proposed. A parametric design tool was developed to study the geometry of two joints that become overlapped in the coiled configuration as a function of the coiling radius and joint radii. Parametric design results are validated through finite element simulations. The proposed design tool provides a high level of design flexibility and is of interest in the spacecraft design process making use of ultra-thin shells.

I. Introduction

Ultra-thin shells are increasingly being used in lightweight structures such as adaptive reflectors and mirrors [1], as well as in aerospace systems where the bending compliance allows to achieve lower packaging volumes, such as deployable booms [2–5], antennas and solar concentrators. Many of these applications require connection elements to either attach shells to each other or to a support structure. Traditional joints for deployable structures are quasi-rigid elements with defined degrees of freedom, connected to stiff members of the structure [6–8]. More recently, compliant joints have been proposed as lighter, smaller and potentially cheaper alternative for joining separate members of a deployable structure. Compliant joints are continuous structural elements which undergo large deformations to achieve the desired change in shape [9]. Trease et al. proposed large-displacement compliant translational and flexural joints to eliminate the presence of friction, backlash, and wear [10]. Ferraro and Pellegrino studied a self-latching flexural joint made from fiber-reinforced polymers (FRP) to replace mechanical hinges [11]. Footdale et al. proposed a concept for compliant hinges allowing a thin shell structure to deploy into non-planar configurations [12].

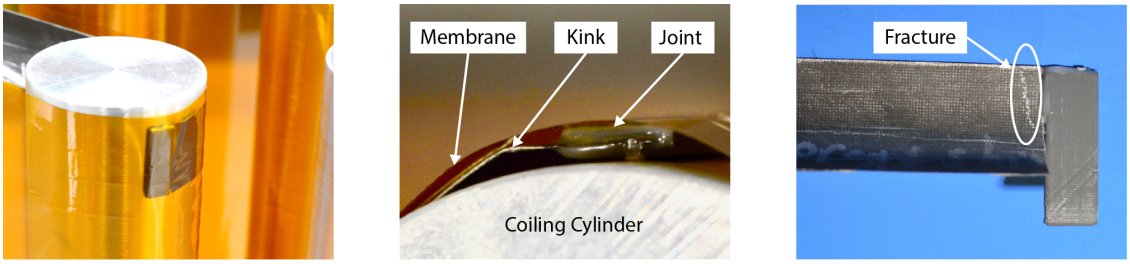

(a) Coiling of a generic joint (b) Top view (c) Coiled sample

Fig. 1 Coiling of a thin-shell connected to a generic solid joint on a cylinder, using a membrane (a). Top view showing a locally high curvature in the thin-shell where the membrane contacts the thin shell (b), leading to failure of the thin-shell material (c).

However, connecting thin shells directly to mechanical joints may lead to localized deformations, stress and mass concentrations. Figure 1(a) shows a Triangular Rollable And Collapsible (TRAC) [13] boom with a web thickness of approximately 400 μm to which a 3D-printed solid joint has been bonded with epoxy resin. A membrane is used to flatten the flanges of the TRAC boom and coil the structure around the cylinder. From the top view shown in Fig. 1(b) a local change in the curvature (kink) is observed at the location where the membrane contacts the thin-shell structure. At

*Postdoctoral Scholar, Graduate Aerospace Laboratories, 1200 East California Boulevard. e-mail: dturk@caltech.edu
†Joyce and Kent Kresa Professor of Aerospace and Civil Engineering, Graduate Aerospace Laboratories, 1200 East California Boulevard, Mail Code 105-50, AIAA Fellow. e-mail: sergiop@caltech.edu

this location the curvature of the thin-shell exceeds its critical value, leading to locally elevated stresses which in turn result in failure on the compression side of the coiled sample, see Fig. 1(c).

This paper presents two strategies for circumventing this effect and more generally addresses the problem of designing and building structural connections between coilable thin-shells with complex shapes. The first strategy involves a stiffness-driven compliant ultra-thin joint, in which the joint gradually transitions in shape and stiffness. This approach requires careful design, as the it must match stiffness requirements in the coiled and the deployed configuration of the structure, where operation loads have to be considered. The second design strategy involves a conforming joint which represents a new category of joint designs for coilable structures. The geometry of a conforming joint is shaped such that it follows the contour of a given geometry. In the particular case presented herein, a conforming joint follows the contour of the coiling cylinder, and connects to a straight region of the thin-shell. The curvature in the interface region is taken by the joint, leaving the thin-shell straight, and thus ideally stress free. A parametric design tool was developed to study the geometry of two joints in the coiled configuration as a function of the coiling radius and joint radii. The design tool is then applied to a structural architecture proposed by the Space Solar Power Project (SSPP) at Caltech [14–16]. This project is developing ultra-light, coilable shell structures made of ultra-thin composites for large deployable space-solar power satellites. Parametric designs are finally validated through finite element simulations.

This paper proceeds as follows. Section 2 presents joint concepts for connecting to thin shells based on requirements which are derived from the current structural architecture proposed in the SSPP. Section 3 presents the parametric design tool for conforming joints including the modelling approach and a parameter study. In Section 4, the design tool is applied to the prototype structure of the SSPP. Section 5 concludes the paper and outlines future work.

II. Design concepts

The requirements for the joints are derived from the structure schematically depicted in Figure 2(a) which is a model of the architecture currently being investigated at Caltech. The space structure may be divided into four identical quadrants. Each quadrant consists of three coilable strips for which a ladder-like architecture has been proposed [16] and realised [17]. A strip consists of two coilable longerons, battens which may be oriented perpendicular or diagonally with respect to the longitudinal axis of the longerons, and four joints at the corners. A tensioned cord which is diagonally deployed along with the structure, acts as a support for the strips. The cross section selected for the longerons is derived from the Triangular Rollable And Collapsible (TRAC) deployable beams and was studied by Leclerc for ultra-thin composite materials [2]. The joint provides a structural and kinematic connection between the longerons and the cord.

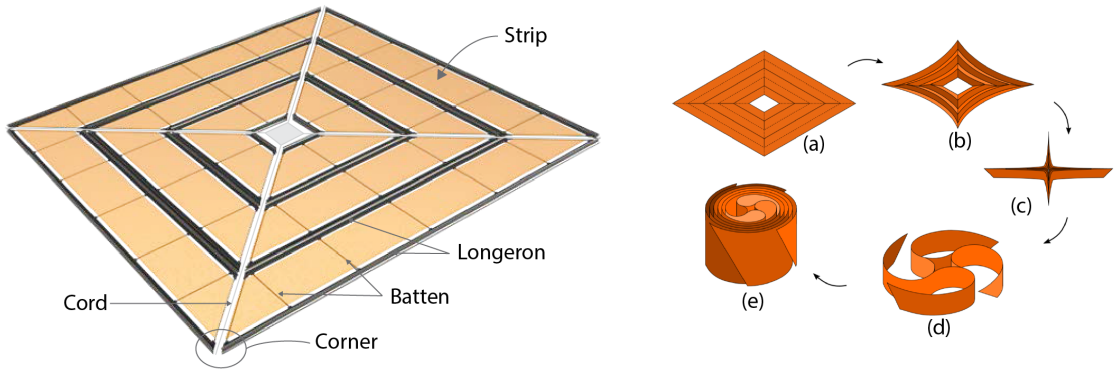

a) Spacecraft architecture

b) Spacecraft packaging scheme

Fig. 2 The spacecraft architecture (a) is based on coilable ladder-like strips and it is Z-folded to a star-shape and coiled for packaging (b) [14, 17].

Figure 2(b) shows the proposed high-efficiency packaging scheme for the space structure [14]. In this packaging scheme, the structure is first folded between the strips, alternating between mountain and valley folds until reaching a star-like shape (a – c). In the next step, the structure is wrapped into a compact packaged cylindrical form (d-e). Based on the proposed structural architecture and its packaging scheme, the following structural and kinematic joints requirements are derived:

- Load-carrying: The joint has to provide a structural connection between the longeron and the cord which acts as a support for the strip under in-space loading conditions such as inertial and solar pressure.
- Foldable: The joint should not fail during packaging and deployment. As the longeron is folded, the joint must undergo compatible deformations without damaging the thin-shells.
- Coilable: The folded structure is coiled for packaging, and the joints have to accommodate the coiling deformation without damaging the thin-shells.
- Rotation about cord-axis: During folding and deployment, the strips rotate about the cord axis which the kinematics of the joint must allow for without over-constraining the strip.
- Ultra-thin: In order to achieve a minimal packaging volume, each component of the joint should be as thin as possible.
- Ultra-light: The joints should be lightweight to reduce the mass of the structure and thus minimize cost of launch and inertia for in-space maneuvers.

A. Preliminary design

A preliminary joint concept is proposed to study the joint geometry and to understand the challenges of connecting stiff elements to thin shells. The joint consists of an assembly of separate elements including a shaft, two stoppers and a 3D-printed interface element, see Fig. 3(a). The 3D-printed hinge elements rotate around the shaft. The kinematics of a revolute joint are realized, as the stoppers define the position of the assembly on the cord and constrain translations in the cord direction. The design freedom of additive manufacturing (AM) is used to integrate the necessary positioning features into the interface [18]. The longeron is connected to the interface through a curved slot with a width of 1.4 mm which follows the contour of the longeron. In addition, two 5 mm long cylinders are integrated into the 3D-printed interface element. In this particular design, the diagonal batten consists of a pultruded CFRP tube with 3 mm outer and 2 mm inner diameter. It is connected to the interface using a cylindrical pocket with a nominal inner diameter of 3.6 mm. A feature to position a metallic sphere is integrated on the flat surface of the interface. The sphere is used as a reference element for shape measurements of the assembled structure.

The interfaces are produced with Selective Laser Sintering (SLS), an AM technique which allows to produce complex shapes without requiring support structures [19]. However, for the particular design embodiment presented herein, a few design constraints have to be considered, including a minimal wall thickness of approximately 0.6 mm, minimum feature size of approximately 1 mm and a minimum gap size of 1.4 mm. Two pins with a nominal diameter of 1.4 mm are located on the lower side of the interface. They are used to position the interface precisely in relation to the overall structure. Adhesive epoxy is then injected through the injection ports into the interface using a syringe. The adhesive cures at room temperature forming a connected structure. Refer to [17] for more detailed information on the manufacturing and assembly of the SSPP spacecraft prototype structure.

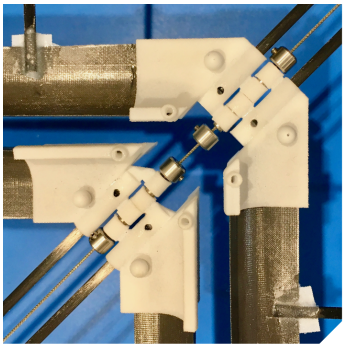

(a) Preliminary joint design

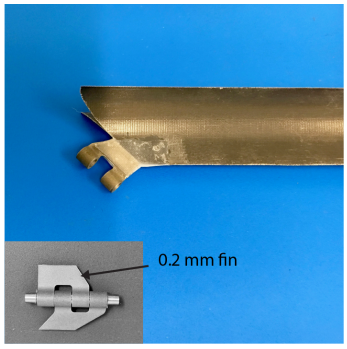

(b) Compliant joint design

(c) Longeron coiled on the compliant joint

Fig. 3 Kinematic joint designs connecting to thin-shells. (a) displays a 3D-printed joint with integrated pockets and slots to host the shell and the diagonal batten. (b) shows a compliant double-strap joint consisting of a steel hinge with a 0.2 mm fin which is fabricated with EDM and two adhesively bonded glass-fiber doublers. During spacecraft packaging, longerons are coiled on top of each other, which results in local buckling of the longeron for this particular design (c).

B. Compliant joint design

Figure 3(b) shows a compliant joint design consisting of an ultra-thin double-strap interface between a steel part and the composite longeron. The steel element is a precise structural element with two cylindrical features serving as hinges on a shaft. In addition, a 0.2 mm thin fin provides the adhesive bonding surface. The steel hinge is manufactured using Electrode Discharge Machining (EDM), a manufacturing technique allowing to produce highly accurate parts with small features from a various range of space-qualified metal alloys. Two pre-cured glass-fiber prepreg layers are cut to net-shape and bonded with epoxy resin at room temperature to the web of the longeron and the fin surface to form a double strap connection. The resulting multi-material joint is a thin and lightweight structural connection with a certain degree of compliance. Figure 3(c) shows a coiled configuration of such an element with an additional longeron coiled on top of the joint, to assess the interaction between the joint and a longeron coiled on top of it. This interaction is required in the packaging sequence of the SSPP spacecraft concept. From this coiling experiment, we can identify local buckles appearing in the upper longeron which is a result of the outer shape of the joint. This experiment reveals that in addition to the requirement of coiling the interface without failure, conforming of the subsequent longeron is of importance to achieve an overall satisfactory design. As a consequence, the outer shape of the joint should guide the subsequent longeron in a way to avoid buckling and failure.

C. Conforming joint design

The key idea of the conforming joint shown in Fig. 4 is to design the shape (contour) of the connection element with the goal to minimize stress concentrations in thin-shells. In this particular case, we want to design the shape (i) of the longeron to which the joint is connected and (ii) the shape of the longeron which is coiled on top of the joint. By designing a curvature which is equal to the curvature of the coiling cylinder at the lower part of the joint, the interface section of the longeron remains straight, see Fig. 4(b). As a consequence, the interface section of the longeron-joint connection ideally remains stress-free in the coiled configuration and high stresses as observed in Fig. 1(b) are avoided.

As previously described, the packaging scheme of the spacecraft requires multiple longerons to be stacked and coiled on top of each other. Therefore, the outer shape of the joint must also be controlled in order to avoid stress concentrations and local buckles potentially resulting in material failure. The outer contour of the joint should be designed such that a superimposed curve is tangential to the respective coiling radii and guided along the joint shape without reaching a radius of curvature exceeding the critical value for material failure, see Fig. 4(c).

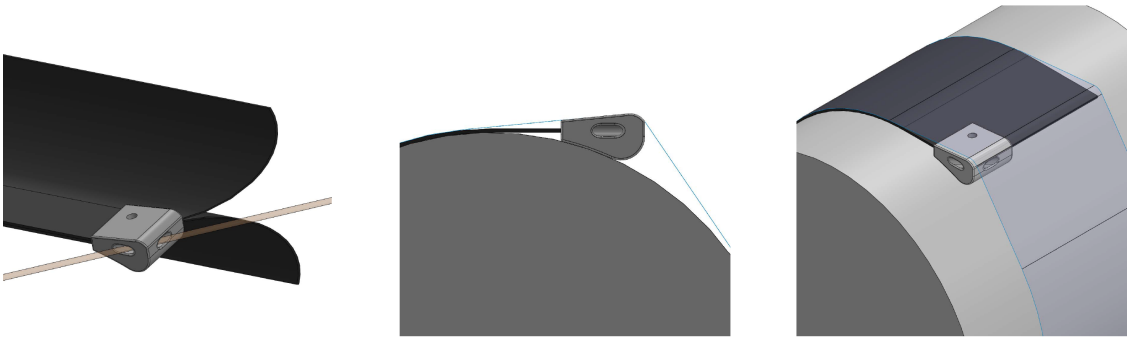

(a) Deployed configuration (b) Coiled configuration, side view (c) Coiled config., isometric view

Fig. 4 The conforming joint is bonded to the web of the longeron (a). In the coiled configuration, a section of the longeron remains straight (b) to avoid stresses at the interface. The joint should provide a conforming contour to the membrane or the longeron being coiled on top of the joint (c).

D. Design evaluation

Table 1 qualitatively compares the two design concepts for joining deployable thin shell structures, described in Subsection II.B and II.C. Key evaluation criteria include a low joint weight for cost-effective operation in space applications. Moreover, the joint should be thin, as the joint height directly impacts the packaging efficiency of the structure. Related to the joint height is its impact on the coiling behavior of subsequent longerons. This criteria will

Table 1 Qualitative design concept evaluation.

Criteria	Compliant Joint	Conforming Joint
Lightweight	+	+
Thinness	+	o
Low impact on coiling behavior	-	+
Structural reliability	o	+
Manufacturing effort	-	+

be considered in more detail in the next section, where we consider the joint height, the arc length of the impacted longeron section on the coiled cylinder, and the stresses in the longeron which is coiled on the joint. In addition, as for any space application a high degree of structural reliability is required. Finally, a future spacecraft with dimensions of approximately 20 by 20 meters will require a large number of connection elements, which is why the manufacturing process should be cost-efficient with reproducible quality. The concepts are qualitatively evaluated where + is advantageous, *o* neutral, and − denotes a negative assessment of the concept towards a specific criterion.

Both concepts are lightweight, depending on material selection, area. It should be noted, that the amount of adhesive may significantly contribute to weight accumulation. The compliant joint design is comparably thin in the region of the fin, but due to the shaft providing the kinematic surfaces a total height of 5 mm is reached, which in the context of ultra-thin structures may be significant. As we will see in the next section, the height of the conforming joints varies depending on the coiling radius R and the allowable joint radius r. Figure 3(c) shows that the impact of the compliant joint on the coiled longeron is disadvantageous for structural and packaging reasons, while the conforming joint is *designed* to control the shape of the coiled longeron. In fact, this is one key argument for further pursuing this type of concept in the next section of this paper. The second argument is the structural reliability of the conforming joint. As described earlier, the interface region between the thin-shell and the joint remains stress-free in the final state of the coiled configuration. In the compliant joint design, the deformation is not avoided in the critical interface region, instead additional design complexity is added. Finally, manufacturing compliant joints is a laborious and multi-stage process involving curing of the doublers, manufacturing the shaft and the hinge. In addition, the process of bonding the doublers to the longeron and the hinge requires a precise jig to align the longeron edge with the hinge edge. Also, the quality control of such complex multi-material bonded joint may be difficult to achieve. The conforming design on the other hand uses a slot with a defined edge in which the longeron is inserted and aligned. Similar to the preliminary design concept, an injection port is provided to bond the two components. The manufacturing of additional connecting elements such as doublers is not necessary. For all these reasons, the next section addresses the parametric design of conforming joints.

III. Parametric design tool for conforming joints

During packaging, two joints of a same corner rotate around the cord axis and become overlapped in the coiled configuration. We therefore have to simultaneously design for a pair of joints to assess the interaction of a thin-shell which is coiled on top of the corner. A parametric design tool to generate the contour geometry of two dependent joints as a function of the coiling radius R and the joint radii r_i of the joint i is developed (Fig. 5). A parametric design tool is desirable because the local coiling radius varies depending on the location of the joint in the packaged configuration of the spacecraft. In addition, multiple strips with joints attached to the corners are stacked, resulting different radii as a function of the strip number in the spacecraft. In general, the further away a strip is located from the coiling center (spacecraft hub), the bigger its coiling radius. But even for the same strip, the joint locations vary. The parametric design tool addresses the following concurring goals:

- Provide an outer contour to which a curve can conform.
- Provide a geometry to host the longeron and the elliptical bore hole for the cord.
- Minimize joint height for maximal packaging efficiency.
- Maximize joint radius to minimize stress concentration in over-coiled longeron.
- Minimize joint area which to reduce joint weight.
- Consider manufacturability through appropriate wall thickness selection.

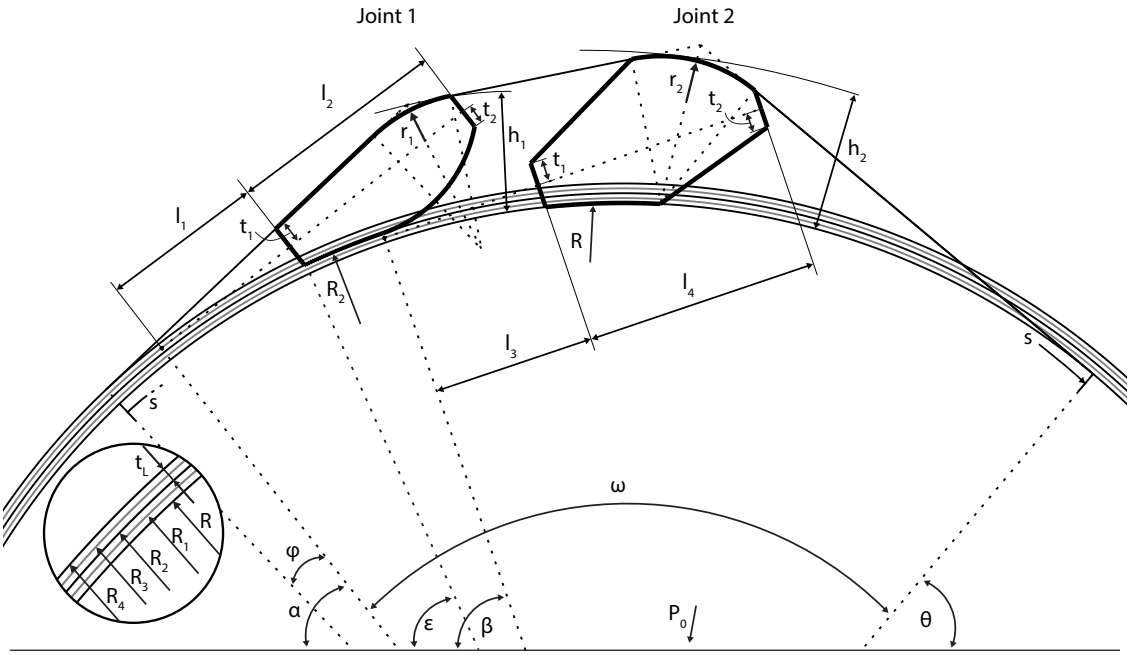

Fig. 5 Parametric design of two conforming joints located on a coiling cylinder and a membrane which is used to flatten and package the structure.

A. Parametric model description

A parametric model with three hierarchical levels was developed. The first level comprises the modeling of the inner skeleton of Joint 1, which mainly depends on the inner packaging requirements to host the longeron and the cord, and positioning references such as the angle α and the coiling radius R. The second hierarchical level consists of the modeling of Joint 2 which is similar to Joint 1. However, the location of Joint 2 is dependent on the location of Joint 1 which is defined by the angle β. The inner skeleton of Joint 2 is constructed similarly to the one of Joint 1. Level 3 of the model generates the outer contour of a membrane or a longeron which is coiled on the two joints. The shape of the outer contour is crucial to assess the packaging efficiency of the structure, as well as to allow the subsequent longeron to be coiled on top of the assembly without structural failure. In particular, the radii r_1 and r_2 of Joint 1 and 2, respectively, are key parameters which determine local coiling radii of the subsequent longeron. In addition, geometric constraints such as tangency of the outer contour with the coiling radius or the longeron radius are defined at this level of the parametric model.

The tool uses vectors and geometric relations to generate the parametric geometry and was implemented in MATLAB R2018a. In the following the key geometric relations are elaborated. Refer to Table 2 for a full list of the parameters included in the model. From geometry, the following relations are obtained and shown in Fig. 6:

$$\mathbf{v}_1 = R_3[-cos(\alpha), sin(\alpha)] \tag{1}$$

$$\mathbf{v}_2 = l_1[sin(\alpha), cos(\alpha)] \tag{2}$$

$$\mathbf{v}_3 = t_1[cos(\alpha), -sin(\alpha)] \tag{3}$$

$$\mathbf{v}_{03} = \mathbf{v}_1 + \mathbf{v}_2 + \mathbf{v}_3 \tag{4}$$

$$\|\mathbf{v}_{03}\| = R_2 \tag{5}$$

$$\mathbf{v}_4 = -\mathbf{v}_3 \tag{6}$$

$$\mathbf{v}_5 = l_2[sin(\alpha), cos(\alpha)] \tag{7}$$

$$\mathbf{v}_6 = t_2[cos(\alpha), -sin(\alpha)] \tag{8}$$

$$\mathbf{v}_7 = -\mathbf{v}_6 \tag{9}$$

$$\mathbf{v}_8 = R_4[-cos(\alpha - \phi), sin(\alpha - \phi)] \tag{10}$$

ϕ is unknown, but the outer contour should be tangent to R_4 which is equal to $\mathbf{v}_8$ being orthogonal to $\mathbf{v}_9$. Therefore,

$$\mathbf{v}_9 \cdot \mathbf{v}_8 = 0 \tag{11}$$

Next, the lower fillet of Joint 1 is defined. The purpose of the fillet is to avoid stresses concentrations in the thin shell which is connected to Joint 2. Therefore, an arc tangential to R_2 with a starting point at the tip of $\mathbf{v}_{10}$ is constructed. To compute the center of the arc, the length of $\mathbf{v}_{11}$ and $\mathbf{v}_{12}$ must be equal. In addition, $\mathbf{v}_{10}$ and $\mathbf{v}_{11}$ must be co-linear:

$$\|\mathbf{v}_{11}\| = \|\mathbf{v}_{12}\| \tag{12}$$

and

$$\mathbf{v}_{11}\mathbf{v}_{12} = \|\mathbf{v}_{11}\|\|\mathbf{v}_{12}\| \tag{13}$$

These equations define the parametric inner skeleton of Joint 1 in dependence of the coiling radius R, the thickness of the longeron t_L, the joint thicknesses t_1 and t_2, and a positioning parameter α. In the next step, we can construct the parametric geometry of Joint 2. We define the angle β to locate Joint 2 on the coiling cylinder. To keep a constant spacing between the joints for varying values of R, β is expressed as a function of a constant, α, and R (c.f. Table 2). Note, that the inner skeleton of Joint 2 is independent, only its location is dependent on the location of Joint 1. The inner skeleton can now be determined in the same manner as previously shown for Joint 1, which is why it is not further elaborated here.

In step 3, we determine the outer contour, which is dependent on the coiling radius and on the geometry of both joints. Therefore we determine $\mathbf{v}_{13}$ and $\mathbf{v}_{14}$ such that $\mathbf{v}_{13}$ is orthogonal to $\mathbf{v}_{14}$ and that the norm of $\mathbf{v}_{13}$ equals R:

$$\mathbf{v}_{13} \cdot \mathbf{v}_{14} = 0 \tag{14}$$

and

$$\|\mathbf{v}_{13}\| = R \tag{15}$$

Next, we determine the center of the radius r_2 of Joint 2 which is defined by $\mathbf{v}_{15}$ and the supporting angle θ such that:

$$\mathbf{v}_{15} = -r_2[cos(\theta), sin(\theta)] \tag{16}$$

This equation implies that $\mathbf{v}_{15}$ and $\mathbf{v}_{13}$ are parallel. The radius r_2 is a variable which is maximized, given the output boundaries such as joint height.

To find the second point of the arc, we define a vector $\mathbf{v}_{16}$ such that:

$$\|\mathbf{v}_{16}\| = r_2 \tag{17}$$

In addition, we define $\mathbf{v}_{17}$ pointing from $\mathbf{v}_{16}$ to $\mathbf{v}_7$ of Joint 1 such that:

$$\mathbf{v}_{16} \cdot \mathbf{v}_{17} = 0 \tag{18}$$

Extending the straight line of the outer contour as defined by $\mathbf{v}_{17}$ and $\mathbf{v}_{14}$ should intersect with the center line of r_2 to equalize the angle between $\mathbf{v}_{16}$ and the center line and $\mathbf{v}_{15}$ and the center line. We construct a vector $\mathbf{v}_{18}$ and $\mathbf{v}_{19}$ with equal length such that:

$$\mathbf{v}_{18} \cdot \mathbf{v}_{16} = 0 \tag{19}$$

and

$$\mathbf{v}_{19} \cdot \mathbf{v}_{15} = 0 \tag{20}$$

with

$$\|\mathbf{v}_{18}\| = \|\mathbf{v}_{19}\| \tag{21}$$

Repeating this approach for Joint 1 will determine r_1 such that the circular arc is tangential to $\mathbf{v}_9$ and $\mathbf{v}_{17}$.

In the final step, the output parameters are defined. The arc length s is defined as the arc length of R and the angle ω between $\mathbf{v}_8$ and $\mathbf{v}_{13}$.

$$s = \omega R \tag{22}$$

The height of Joint 1 and 2 denoted by h_1 and h_2, respectively are evaluated using a point P_1 and P_2 that are located on the arc of Joint 1 and 2, respectively. The method for constructing these points is exemplified on Joint 2. There is a vector $\mathbf{v}_{20}$ with a length equal to r_2:

$$\|\mathbf{v}_{20}\| = r_2 \tag{23}$$

In addition, $\mathbf{v}_{20}$ is co-directional to a vector $\mathbf{v}_{21}$ relating the origin to the center of the arc such that:

$$\mathbf{v}_{20} \cdot \mathbf{v}_{21} = \|\mathbf{v}_{20}\|\|\mathbf{v}_{21}\| \tag{24}$$

Finally, the height of Joint 2 is defined as:

$$h_2 = \|\mathbf{v}_{20} + \mathbf{v}_{21}\| - R \tag{25}$$

The height of Joint 1 is computed similarly:

$$h_1 = \|\mathbf{v}_{22} + \mathbf{v}_{23}\| - R \tag{26}$$

The surface area of a joint is computed as a union of finite surface pieces which do not overlap. For example, the joint surface area is the union of a rectangle, two triangles, and two arcs.

B. Parameter study

Figure 7 shows the variation of the key output parameters with the input variables such as the coiling radius R ranging from 20 to 80 mm and the radius of Joint 2, r_2, ranging from 6 to 8 mm. In Fig. 7(a), the variation of the joint radius 1, r_1, is shown with R for different values of r_2. The dependency of r_1 from r_2 is significantly pronounced for small values of R. For $R = 20$ mm, an increase of r_2 by 0.5 ranging from $6 - 8$ yields an increase of r_1 by $1, 1.7, 3.4$ and 12.3. However, as the coiling radius R increases, the dependency of r_1 from r_2 decreases and becomes approximately constant. In general, for a given value of R, increasing r_2, increases r_1. In addition, it should be noted that for most values of R, $r_2 > r_1$. One exception where $r_2 < r_1$ consists of the configuration where $r_2 = 6$ mm and $R < 25$ mm, which may be excluded from the design space, depending on the user-defined value for r_{min}. Figure 7(b) shows the variation of the joint height h_1 and h_2 for different values of r_2 with R. In general, the height decreases as R increases. As the coiling radius increases, the smaller gets the required change in direction of the outer contour for a given joint, see also Fig. 8. Hence, the height decreases with increasing R. Note that h_1 is independent of r_2 which is a consequence of the hierarchy within the parametric model, as h_1 is defined prior to r_2. In addition, note that for R within [20 80] , $h_2 > h_1$. For h_2, a similar trend to $r_1(R, r_2)$ is observed, albeit less pronounced. The height of Joint 2 increases for a given R with increasing r_2. This effect becomes less important with increasing R. This figure also shows that a small joint height which is desired for packaging, is contradictory with a large joint radius, which in turn is desirable to minimize local stress concentrations in the longeron coiled on top of the joint. For example, Fig. 8(c) shows a design for $R = 35.4$ mm where the driving height is the one of Joint 2 which amounts to $h_2(R = 35.4, r_2 = 6) = 5.6$ mm. Figure 8(d) shows the same design for the radius of Joint 2 increased to $r_2 = 8$ mm which results in $h_2(R = 35.4, r_2 = 8) = 5.9$ mm. The addition of heights over multiple accumulated corners may have to be considered during packaging. However,

Table 2 Variables, fixed, dependent and output parameters and their relations in the model.

Term	Symbol	Range	Unit
Variables			
Coiling radius	R	20-80	mm
Radius of Joint 2	r_2	6-8	mm
Fixed parameters			
Angle between horizontal and tangent to R_3	α	0.9598	rad
Min. joint thickness to host longeron	t_1	0.95	mm
Min. joint thickness to host cord	t_2	0.8	mm
Length of Joint 1	l_2	9	mm
Length of Joint 2	l_4	9.66	mm
Thickness of longeron	t_L	0.4	mm
Dependent parameters			
Radius of neutral axis of longeron 1	R_1	$R + 0.5 * t_L$	mm
Radius of top plane of longeron	R_2	$R + t_L$	mm
Radius of neutral axis of longeron 2	R_3	$R + 1.5 * t_L$	mm
Radius of top plane of longeron 2	R_4	$R + 2 * t_L$	mm
Spacing between joints	β	$(cst + \alpha * R)/R$	rad
Length l_1	l_1	$f(\alpha, t_1, R_2, R)$	mm
Angle between joint midplane and membrane	ϕ	$f(\alpha, R_4, t_1, l_1)$	rad
Angle between joint edge and horizontal	ϵ	$f(\alpha, R_4, t_1, l_1)$	rad
Length l_3	l_3	$f(R_1, \beta, t_1, R)$	mm
Angle of affected area	ω	$\angle \mathbf{v}_8\mathbf{v}_{11}$	rad
Output parameters			
Height of Joint 1	h_1	$\|\mathbf{v}_{20} + \mathbf{v}_{21}\| - R$	mm
Height of Joint 2	h_2	$\|\mathbf{v}_{22} + \mathbf{v}_{23}\| - R$	mm
Area of Joint 1	A_1	$area(Joint\ 1)$	mm^2
Area of Joint 2	A_2	$area(Joint\ 2)$	mm^2
Radius of Joint 1	r_1	$\|\mathbf{v}_{22}\|$	mm
Affected arc length	s	$\omega * R$	mm

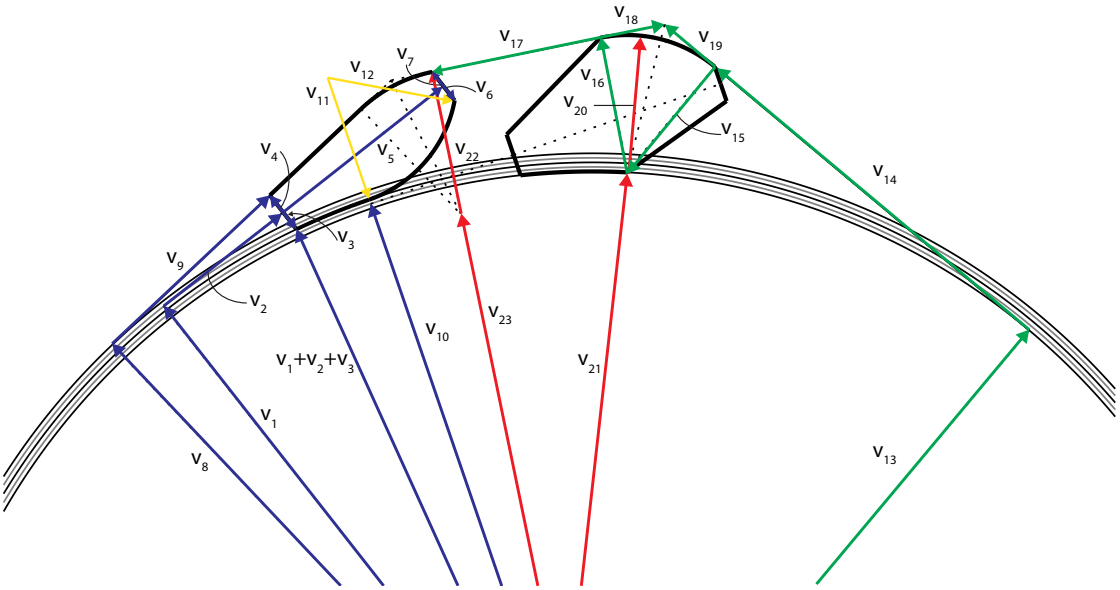

Fig. 6 Vector-based generation of the parametric geometry showing vectors to compute Joint 1 and the outer contour.

as R increases, a change in r_2 from 6 to 8 does not significantly affect h_2 as the effect gets less pronounced with large R. With this graph, it becomes clear that R and h are concurrent parameters considering the packaging efficiency of a spacecraft. Large values of R yield small and packageable joints, but reduce the overall packaging efficiency. In contrast, small values of R increase the overall packaging efficiency, but necessitate larger joints in order to keep the longeron-joint interface stress free.

Figure 7(c) shows the variation of the surface area A_i of each joint with R and discrete values of r_2. In general we observe that for the given range of R and r_2, $A_1 < A_2$. As the joint height is a key factor driving the surface area, it is not surprising, that similar trends are observed. For small coiling radii, the surface area of the joints increases as a result of a larger values for joint heights and joint radii, which relate to a more accentuated redirection of the outer contour. In contrast, with larger coiling radii, the dependency of the surface area on R decreases. This is expected, as the changes in joint height and radii decrease with increasing R, making the overall design less sensitive to parameter variations. Therefore, with increasing R, A_i decreases. Moreover, A_2 depends on r_2. In general, for a given value of R, larger values of r_2 yield larger surface areas, with the exception of R close to 20 mm where the model limit is reached, see Fig. 8(b). In addition, A_2 is more sensitive to variations of r_2 than A_1. The joint area may be considered as an indicator for the joint weight and therefore ideally is minimized. Finally, in Fig. 7(d), the arc length s is plotted over R. The arc length depends on R and the angle ω (see Fig. 5) which denotes the angle between the points where the outer contour is tangent to either R and R_4. s indicates a range in which the coiled geometry is disturbed by the joint. Outside of the arc s, the outer contour ideally conforms to its associated radius. Small coiling radii yield smaller arc lengths, although disturbances with greater joint height. With increasing R the arc length s also increases, yielding a longer but probably less critical region of disturbance, as the joint height decreases with R.

C. Model limitations

The parametric model has a few limitations. First, the variable range is limited from $R = [20\ 80]$ mm and $r_2 = [6\ 8]$ mm. To generate physical designs for coiling radii $R > 80$, we must reduce $r_2 < 8$. As seen in Fig. 8(g), it is possible to increase R up to 130 mm at the expense of decreasing r_2 from 8 to 6 mm. In some cases the joint may be located on a flat section of the packaged structure, which equals $R \rightarrow \infty$.

In this study, a certain number of fixed parameters including joint lengths l_1, l_2 as well as minimum joint thicknesses t_1, t_2 are given. However, dependent on the selected manufacturing technique t_1, t_2 may increase or decrease. For example, for laser sintering and melting additive manufacturing process, a minimum wall thickness in the range of 0.6 to 1 mm may be required as a minimum wall thickness, mainly dependent on the process parameters, the part geometry and

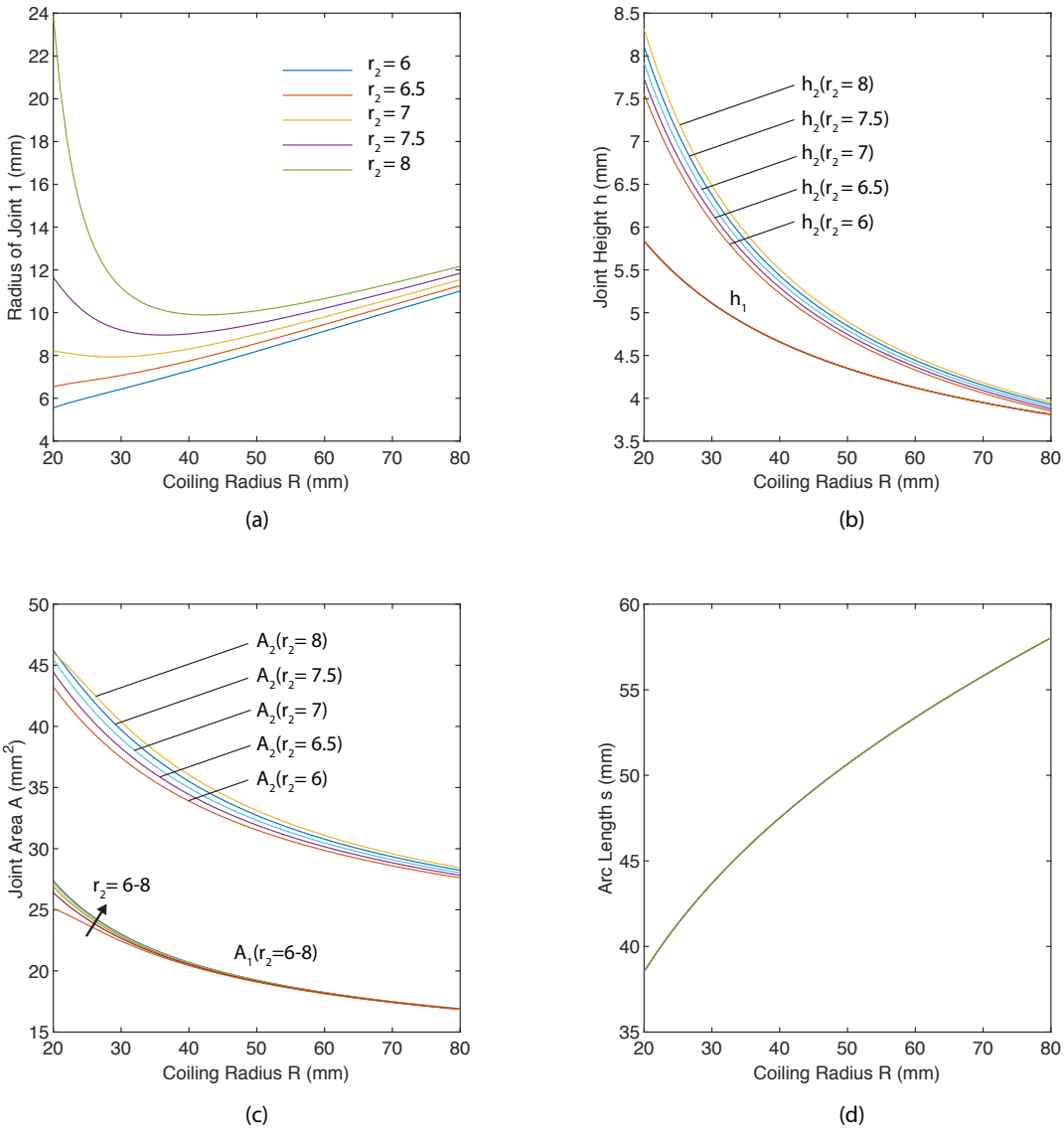

Fig. 7 Parametric model output. (a) shows the dependency of joint radius 1 r_1 of joint radius 2 r_2 over the coiling radius R. As R increases, the dependency of r_1 on r_2 decreases. For values of $r_2 \leq 6.5$, r_1 increases with increasing R. For configurations with high values of r_2 and small R, r_1 tends to increase significantly reaching the limit of physically plausible designs. (b) shows the variation of the joint height h_i for different values of r_2 with the coiling radius R. In general the height decreases with increasing R, and increases with increasing r_2.Note that h_1 is independent from r_2. In (c) the joint area A_i is related to R for different values of r_2. In general the joint area decreases with increasing R, and increases with large values of r_2. The area of Joint 1 is not as dependent on r_2 as it is for A_2. (d) shows the arc length s over R.

the material. Using electrode discharge machining, thicknesses as thin as 0.2 mm may be achieved for high performance alloys. Therefore, the contribution of t_i to the overall joint thickness will be studied in future. Also, they may not be equal, which would add flexibility to the design space.

In this work, we have not considered the mechanical *stability* of the joints. In particular Joint 1 may tilt forward during packaging, which may lead to a different packaged contour geometry. This effect is considered to be small for the following reasons. First, the joint is connected to the longeron which constrains the degree of rotation. Second,

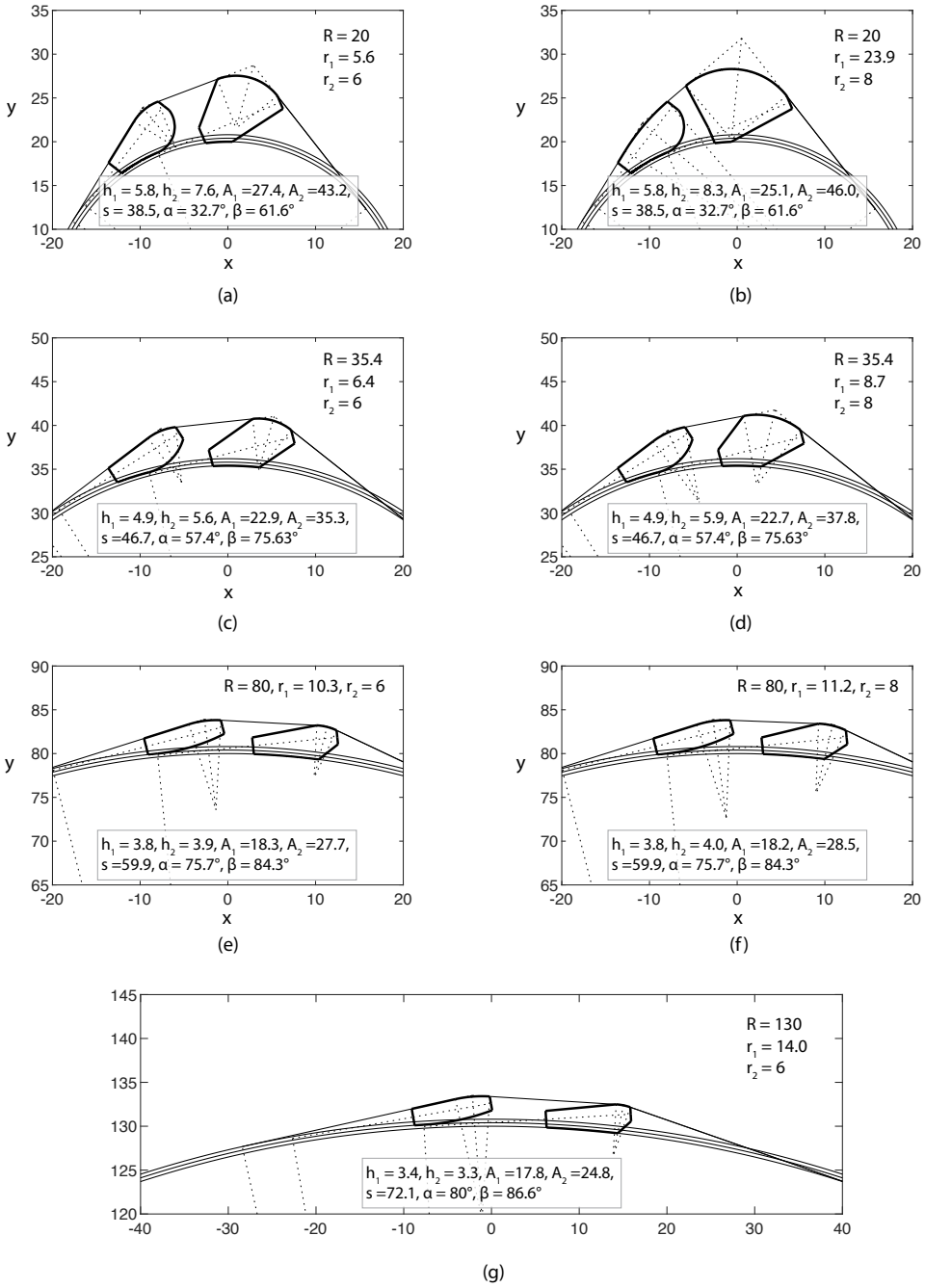

Fig. 8 Design examples for different values of the coiling radius R, and the radius of Joint 2 r_2 as input parameters. (a) and (b) show model limits with $r_1 < r_2$ and physically possible but unsuitable designs. (c) and (d) show design examples for $R = 35.4$ mm which is a plausible value for a coiling radius of a given corner in the spacecraft packaging concept. (e) and (f) show upper limits for a configuration with $R = 80$ mm and $r_2 = 8$ mm. The model can be extended to values of $R > 80$ at the cost of reducing r_2, which is shown for a physically plausible design example with $R = 130$. h_i, A_i denote the height and the area of Joint 1 and 2, respectively. s is the arc length along R which is affected by the joint design, α and β are positioning and joint spacing parameters. Units are in mm, mm^2 and degrees.

Joint 1 is located on top of a compliant longeron, which leads to this effect being moderate. To reduce this effect, we may allow the lower longeron to undergo an infinitesimal deflection, or increase the joint spacing. In future, a stability criterion may be considered.

In the presented model, the spacing of the joints is given by $\beta - \alpha$, where β denotes the angle between the horizontal and the tangential to R_1. If $\beta \rightarrow \epsilon$, where ϵ is the angle between the horizontal and the left-hand side of Joint 1, the lower arc length of Joint 1 approaches 0. In this case, the spacing must be increased. However, increasing the spacing, equals to an increase of the extruded (out-of-plane) dimension, which results in a longer joint. On the other hand, increasing the spacing is advantageous for joint stability.

Finally, for the design embodiment, the critical value of r_i should be determined through simulations and experimentally for the longeron, given the geometry, layup, and material.

IV. Case study

In this section, the design tool is applied to the spacecraft architecture described in [17]. Figure 9 shows a top view of the packaged configuration of the deployable space structure described in Section II. The crosses denote the locations of the strip corners at which the joints are located. From the figure we can see, that the corners are distributed along the packaged structure. Some corners are located on flat sections ($R \rightarrow \infty$) while others are located on curved sections with varying radii. The parametric design tool allows the instant generation of designs with radii matching R. In the following, a corner which is located on a curved section with a coiling radius of $R = 35.4$ mm is selected. The parametric design tool outputs the designs shown in Fig. 8(c) for $r_2 = 6$ mm and Fig. 8(d) for $r_2 = 8$ mm. Design (c) is smaller, and has lower surface area (which relates to lower weight) compared to design (d). It is therefore selected, and the process of coiling a longeron on top of the joints using numerical simulations is studied next.

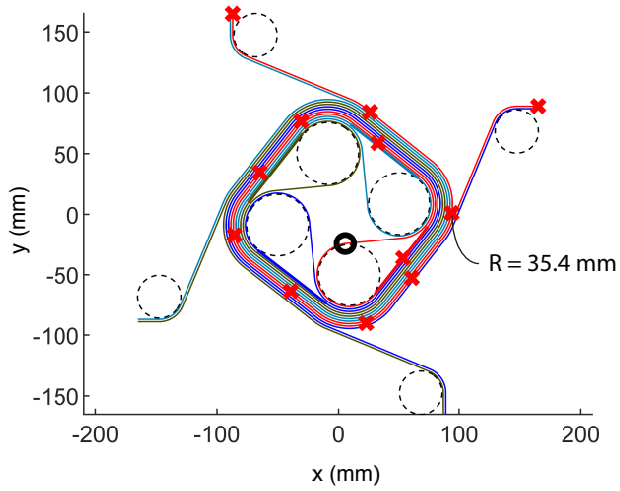

Fig. 9 Joint location for a coiled spacecraft structure similar to the prototype built in [17]. 'x' marks the location of the joints for each strip. The structure is coiled on four cylinders with strips forming tear-drop shapes. Figure courtesy of A. Pedivellano.

Table 3 Material properties.

Term	E_1 (GPa)	E_2 (GPa)	G_{12} (GPa)	ν_{12} $(-)$	t (μm)
Carbon-fiber prepreg	128	6.5	7.5	0.35	30
Glass-fiber prepreg	23.8	23.8	3.3	0.17	35
Membrane	5	5	1.8	0.35	100

A. Numerical simulations

A numerical simulation model was built using the commercially available Simulia Abaqus R2017x software to investigate the quasi-static impact of a thin-shell longeron being coiled over of two joints. The goal of the simulation is to assess the contour of and the stresses in the coiled longeron as a result of the joint geometry. The model includes a 150 mm long composite longeron which is modeled as two separate continuum shell sections which are tied together in the region of the web. The layup of the shell sections is based on [2] and consists of a $[45_g/0_c/45_g]_s$ symmetric laminate, where the subscript g designates glass-fiber plan weave and c carbon-fiber prepreg. Table 3 shows the laminae properties. The joints are modeled as rigid body elements with joint radii of $r_1 = 6.4$ mm and $r_2 = 6$ mm. A membrane is used to flatten and coil the longeron on the cylinder. Isotropic material with properties similar to Kapton are assigned to the membrane which is modeled as a 0.1 mm thin shell. The rigid cylinder has radius of 35.4 mm.

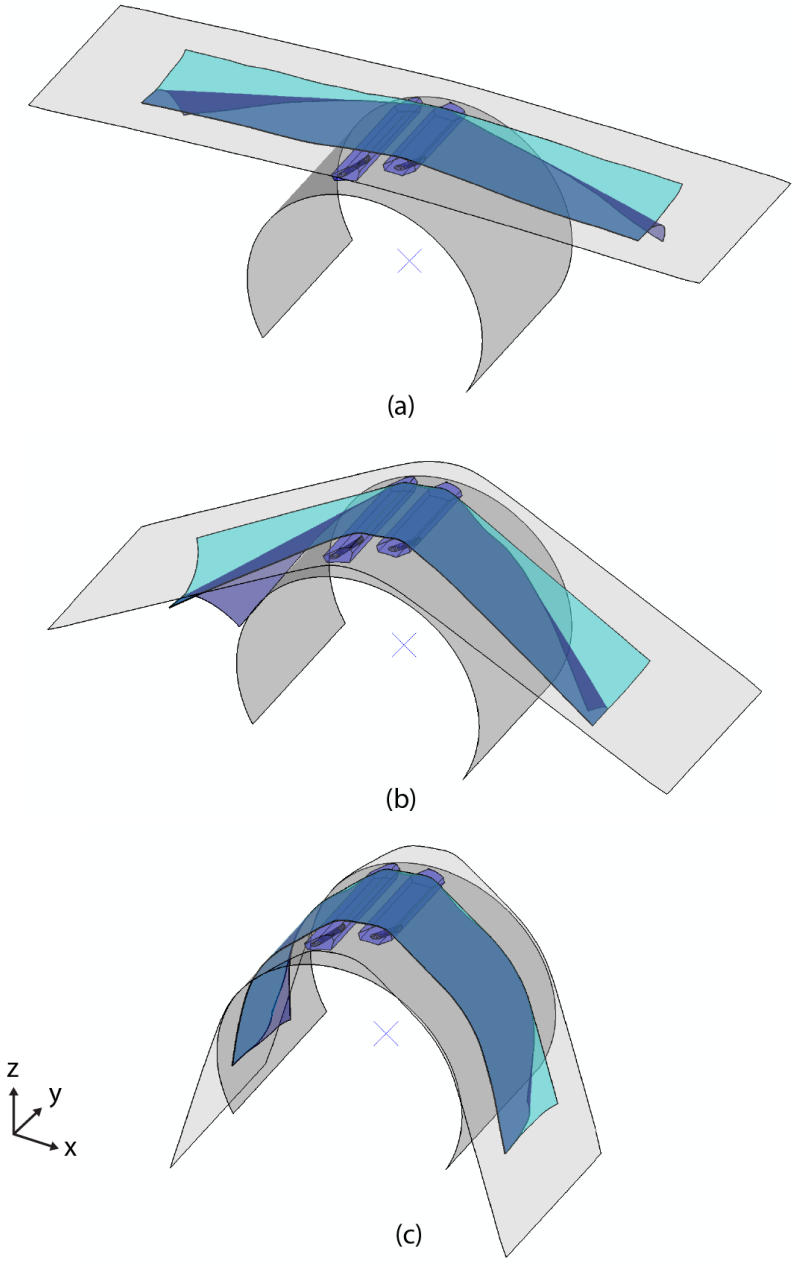

Fig. 10 Simulation sequence. Flattening and coiling a thin-shell longeron on two joints and a cylinder as it is the case in the packaging scheme of the SSPP spacecraft.

In the first step, the membrane is biaxially tensioned by applying a displacement of 1 mm to all four edges. In the next step, an additional displacement condition in the -z-direction is applied to the tensioned membrane. At the same time the cylinder and the joints move upwards until being in contact with the web of the longeron, see Fig. 10(a). At this stage, the upper flange is flattened by the membrane, but the edge of the web of the longeron remains straight. In the next step, the joints and the cylinders are clamped, while the tensioned membrane continuously moves downward, see Fig. 10(b). Note, that boundary conditions are applied only to one root edge of the longeron. However, the pressure load applied by the membrane acts quasi-symmetrically on the longeron. In the final step of the simulation, the membrane moves toward the cylinder while continuing to coil the longeron until reaching its final coiled state, see Fig. 10(c). The simulation model uses a total of 36'000 elements. The membrane is meshed using quadrilateral elements of type S4, the continuum shell elements in the longeron are hexahedral of type SC8R. The cylinder is meshed with S4 elements and the joints use elements of type R3D4 and R3D3. The simulation runs in Abaqus explicit. The element size is reduced in the region where the joint impacts the structure to capture the extreme deformation of the longeron. In this particular region of interest, the element size of the longeron should be smaller than the one of the joint.

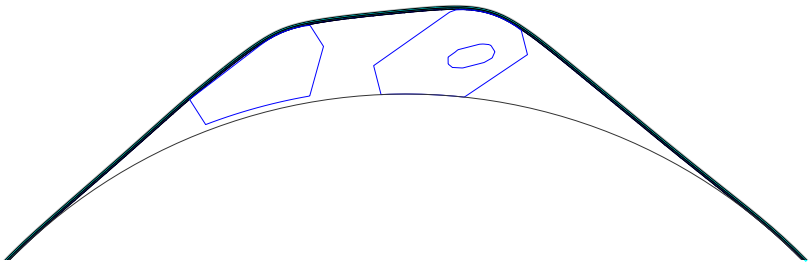

(a) Section view in web

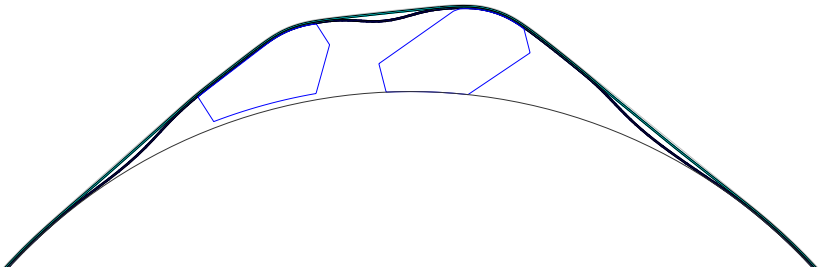

(b) Section view in flange

Fig. 11 Section view showing a conforming longeron at web section and buckling of the flange of lower longeron.

B. Numerical results

The results of the simulation reveal that the longeron conforms particularly well to the outer contour of the joints in the section of the longeron web, which is where the two longeron sections are bonded together, see Fig. 11(a). Periodic buckling of the flange of the lower longeron is observed, see Fig. 11(b). This is a common phenomenon which occurs during coiling thin shells with TRAC cross sections. It is a result of a thickness-effect due to which the lower longeron covers a shorter path compared to the upper longeron [20]. The joint section exhibits a higher curvature which may pronounce this effect.

Figure 12(a) shows the stresses in the bottom ply of the lower longeron in the local 1-direction which is defined along the longitudinal edge of the longeron. Compressive stresses amounting up to $\sigma_{11} = -280.2$ MPa appear in the web section of the longeron which is conforming to the joint radii. These stresses disappear in the flange region, as the flanges are allowed to shear. The lower flange buckling effect is clearly visible in three regions which exhibit elevated tensile stresses amounting up to $\sigma_{11} = 219.3$ MPa. It seems that it is energetically more favorable to form buckles in the lower flange yielding regions with tensile stresses instead of having high compressive stresses in the joint area. Figure 12(b) reports the longitudinal stresses in the topmost ply of the upper longeron. Two regions with significant tensile

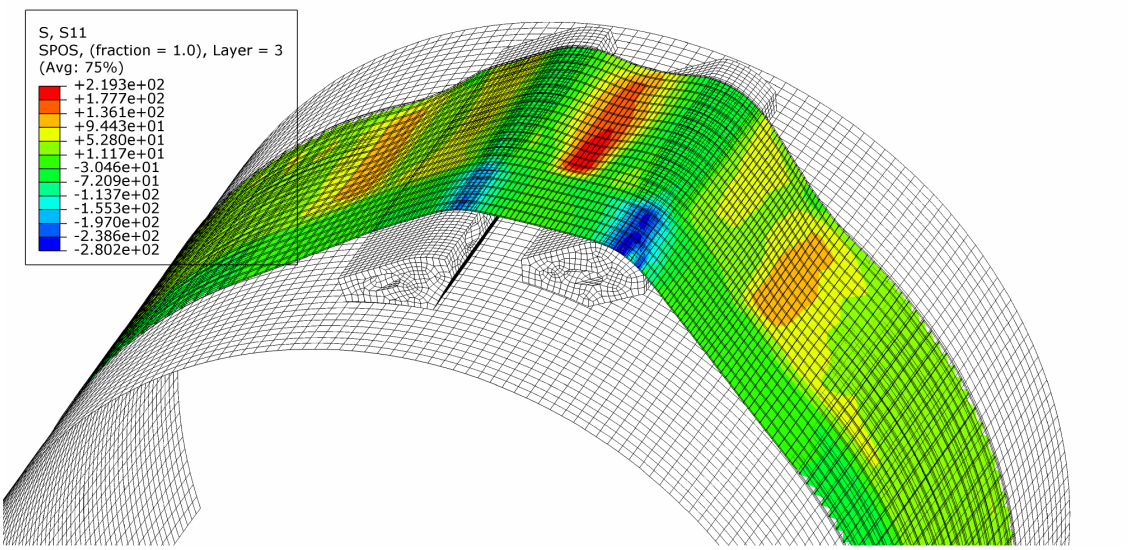

(a) Stresses in the longitudinal direction of the bottom ply in the lower longeron

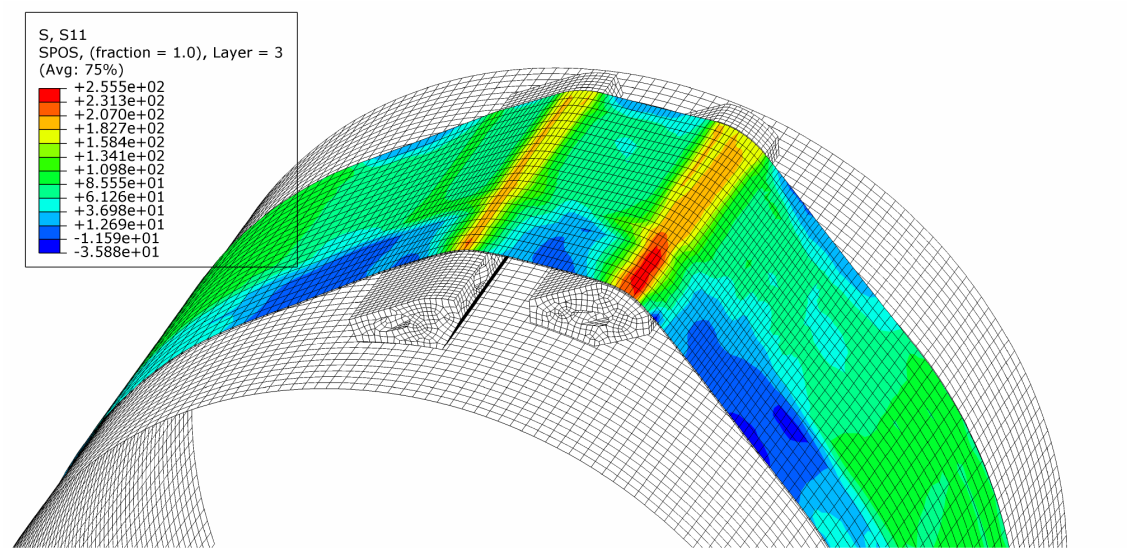

(b) Stresses in the longitudinal direction of the topmost ply in the upper longeron

Fig. 12 Stresses in the local 1-direction of the bottom ply of the lower longeron (a) and of the topmost ply in the upper longeron.

stresses appear at the location of the joint radii across the whole width of the longeron. The maximum tensile stress is located in the web region of the longeron which is conforming to the second joint amounting up to $\sigma_{11} = 255.5$ MPa. Regions with minor compressive stresses are located at the outer edge of the flange and in the web section. In general, the stresses caused by the joint radius $r_2 = 6$ mm are found to be smaller compared to the stresses caused by joint radius $r_1 = 6.4$ mm. A failure criterion for the given laminate an the layup currently is under development, but existing failure criteria for thin-ply composites show compressive and tensile strenghts being larger compared to the ones found in the presented numerical simulation [21]. In future work, the joint radius r_i will be correlated to the stresses found in the longeron which in combination with a failure criterion will provide the designer with values for the critical radius.

V. Conclusions

Designing and building structural connections for ultra-thin shells is challenging and may result in stress concentrations and failure during coiling. In addition, the volume and the stiffness of connection elements induce irregularities and stresses in the packaged structure, potentially compromising the packaging efficiency and the structural requirements. These challenges have been addressed by investigating joints for ultra-thin shells using a geometric approach and numerical simulations. A 3D-printed joint with integrated pockets, a compliant multi-material double strap joint, and a conforming joint were proposed and evaluated. Furthermore, a parametric design tool has been developed for the automated generation of conforming joint designs for the specific problem of coiling a corner of the SSPP spacecraft architecture on a cylinder. Using the coiling radius and the joint radius as input parameters, the model output consists of the joint height, joint area, as well as the disturbed arc length of the coiled region. Lastly, the tool was applied to a specific corner of the SSPP spacecraft and numerical simulations were performed in order to analyze the stresses in the thin shell which is coiled around the specific pair of joints. Future work includes the experimental and numerical study of coiling conforming joints with multiple thin shells being stacked, and the design tool will include the consideration of mechanical stresses in the design generation. The developed design tool and the numerical procedure will help to better understand the effect of packaging solid elements together with thin shells. This procedure is not limited to the packaging of joints and can be generalized to the packaging of critical rigid body spacecraft elements.

Acknowledgments

We thank Dr. Yang Li for advice on the parametric model. We also thank A. Pedivellano for providing the case study. Financial support from the Space Solar Power Project at Caltech is gratefully acknowledged.

References

[1] Steeves, J., and Pellegrino, S., "Ultra-thin highly deformable composite mirrors," *54th AIAA/ASME/ASCE/AHS/ASC Structures, Structural Dynamics, and Materials Conference, Boston, MA*, 2013.

[2] Leclerc, C., Wilson, L. L., Bessa, M. A., and Pellegrino, S., "Characterization of Ultra-Thin Composite Triangular Rollable and Collapsible Booms," *AIAA Spacecraft Structures Conference, SciTech Forum, Grapevine, TX*, 2017.

[3] Block, J., Straubel, M., and Wiedemann, M., "Ultralight deployable booms for solar sails and other large gossamer structures in space," *Acta Astronautica*, Vol. 68, No. 7-8, 2011, pp. 984–992.

[4] Roybal, F., Banik, J., and Murphey, T., "Development of an elastically deployable boom for tensioned planar structures," *48th AIAA/ASME/ASCE/AHS/ASC Structures, Structural Dynamics, and Materials Conference, Honolulu, Hawaii*, 2007.

[5] Herbeck, L., Leipold, M., Sickinger, C., Eiden, M., and Unckenbold, W., "Development and test of deployable ultra-lightweight cfrp-booms for a solar sail," *Spacecraft Structures, Materials and Mechanical Testing*, Vol. 468, 2001.

[6] Norwood, D. C. I., Preliasco, R. J., and Hult, T. D., "Joint for deployable structures," , Dec. 17 1985. US Patent 4,558,967.

[7] Lake, M., Warren, P., and Peterson, L., "A revolute joint with linear load-displacement response for precision deployable structures," *37th Structure, Structural Dynamics and Materials Conference, Salt Lake City, UT*, 1996, pp. 1639–1647.

[8] Hachkowski, M. R., Peterson, L. D., and Lake, M. S., "Friction model of a revolute joint for a precision deployable spacecraft structure," *Journal of spacecraft and rockets*, Vol. 36, No. 4, 1999, pp. 591–598.

[9] Howell, L. L., *Compliant mechanisms*, John Wiley & Sons, 2001.

[10] Trease, B. P., Moon, Y.-M., and Kota, S., "Design of large-displacement compliant joints," *Journal of mechanical design*, Vol. 127, No. 4, 2005, pp. 788–798.

[11] Ferraro, S., and Pellegrino, S., "Self-Deployable Joints for Ultra-Light Space Structures," *AIAA Spacecraft Structures Conference, SciTech Forum, Orlando, FL*, 2018.

[12] Footdale, J., Banik, J., and Murphey, T., "Design developments of a non-planar deployable structure," *51st AIAA/ASME/ASCE/AHS/ASC Structures, Structural Dynamics, and Materials Conference, and Co-located Conferences, AIAA, Orlando, FL*, 2010.

[13] Murphey, T. W., and Banik, J., "Triangular rollable and collapsible boom," , Mar. 1 2011. US Patent 7,895,795.

[14] Arya, M., Lee, N., and Pellegrino, S., "Ultralight structures for space solar power satellites," *AIAA Spacecraft Structures Conference, SciTech Forum, San Diego, CA*, 2016.

[15] Gdoutos, E., Leclerc, C., Royer, F., Kelzenberg, M. D., Warmann, E. C., Espinet-Gonzalez, P., Vaidya, N., Bohn, F., Abiri, B., Hashemi, M. R., Gal-Katziri, M., Fikes, A., Atwater, H., Hajimiri, A., and Pellegrino, S., "A lightweight tile structure integrating photovoltaic conversion and RF power transfer for space solar power applications," *AIAA Spacecraft Structures Conference, SciTech Forum, Orlando, FL*, 2018.

[16] Royer, F., and Pellegrino, S., "Ultralight Ladder-type Coilable Space Structures," *AIAA Spacecraft Structures Conference, SciTech Forum, Orlando, FL*, 2018.

[17] Gdoutos, E. E., Leclerc, C., Royer, F., Türk, D.-A., and Pellegrino, S., "Ultralight spacecraft structure prototype." *AIAA Spacecraft Structures Conference, SciTech Forum, San Diego, CA*, 2019.

[18] Türk, D.-A., Kussmaul, R., Zogg, M., Klahn, C., Leutenecker-Twelsiek, B., and Meboldt, M., "Composites part production with additive manufacturing technologies," *Procedia CIRP*, Vol. 66, 2017, pp. 306–311.

[19] Mueller, B., "Additive manufacturing technologies–Rapid prototyping to direct digital manufacturing," *Assembly Automation*, Vol. 32, No. 2, 2012.

[20] Murphey, T. W., Turse, D., and Adams, L., "TRAC boom structural mechanics," *AIAA Spacecraft Structures Conference, SciTech Forum, Grapevine, TX*, 2017.

[21] Amacher, R., Cugnoni, J., Botsis, J., Sorensen, L., Smith, W., and Dransfeld, C., "Thin ply composites: experimental characterization and modeling of size-effects," *Composites Science and Technology*, Vol. 101, 2014, pp. 121–132.